Nonperturbative treatment of the Thomas mechanism in electron capture

Nobuyuki Toshima
Institute of Applied Physics, University of Tsukuba, Tsukuba, Ibaraki 305, Japan
and Atomic Physics Laboratory, Institute of Physical and Chemical Research (RIKEN), Wako 351-01, Japan

Jörg Eichler*
Bereich Schwerionenphysik, Hahn-Meitner-Institut Berlin, D-1000 Berlin 39, Germany
(Received 18 February 1992)

We present differential and total cross sections for charge transfer in proton-hydrogen collisions at 5, 2.8, and 1 MeV, derived from extensive nonperturbative coupled-channel calculations. We use expansions of target and projectile bound and continuum states of angular momenta up to $l=2$ in terms of Gaussian-type orbitals. Satisfactory convergence is reached. Good agreement is achieved with the experimental data at 5 MeV but not at 2.8 MeV.

PACS number(s): 34.70.+e

I. INTRODUCTION

The theory of electron capture has been discussed extensively in the past decade. There are two main lines of approach to this problem. One of them is the coupled-channel method [1,2], which is usually applied when the velocity of the active electron is smaller than, or comparable to, the projectile velocity. In this method, the time-dependent Schrödinger equation for an electron subject to the potentials produced by nuclei moving along classical trajectories is approximately solved by expanding the total wave function in terms of a truncated set of suitably chosen basis functions. Subsequently, the time-dependent expansion coefficients are determined. This nonperturbative procedure finds its limitation at higher projectile velocities when the interaction matrix elements and their integrands assume an increasingly oscillatory behavior (caused by the translation factor [3]) which renders their numerical evaluation difficult, if not impossible. However, at lower energy, the coupled-channel approach is exceedingly successful [2] in predicting excitation, ionization, and capture cross sections.

The second line of approach, which in a way is complementary, is based on some kind of perturbative treatment and is applicable only when the projectile velocity considerably exceeds the electron velocity. In particular, at asymptotically high, yet nonrelativistic velocities, charge transfer is dominated by a double-scattering mechanism named after Thomas [4], who, as early as 1927, proposed a classical description for electron capture. In the first step of this process, the initially bound electron is scattered off the projectile by 60°, thereby acquiring a speed equal to the projectile velocity. In a second step, the electron is elastically rescattered off the target nucleus by again 60°, so that it travels along with the projectile. The momentum transfer leads to a small deflection of the projectile by the classical Thomas angle [4,5] $\Theta_{\mathrm{Th}}=(\sqrt{3}/2)m_e/M_P$, where m_e and M_P are electron and projectile mass, respectively. Recent classical-trajectory Monte Carlo calculations [6] in which the classical equations of motion are solved rigorously have confirmed the existence of this mechanism.

In 1955, Drisko [7] established the connection of this process with a quantum-mechanical description in a second Born approximation. Since that time, the process has been reconsidered in various degrees of approximations [8–12,14,15] and, above all, has been identified experimentally as a peak in the differential cross section for electron capture [16,17]. This "Thomas peak" indeed occurs at the angle Θ_{Th} (in the laboratory frame) in approximate agreement with theoretical predictions.

Theoretical treatments so far have remained within the framework of second-order perturbation theory, sometimes including higher-order corrections in an approximate fashion. It is implied in the second-order Born approximation [8,9,15] or boundary-corrected Born approximations [10,11,14] that the intermediate state in which the electron propagates between the two collisions is represented by a plane wave or phase-distorted plane waves, respectively. This has the advantage that there is only a single continuum belonging both to the target and to the projectile. However, such a treatment disregards the Coulomb distortion of the electron wave function due to the interaction with each of the nuclei in the reaction zone, which, in principle, might wash out the Thomas peak predicted by perturbation theory. A variety of higher-order theories that take account of the Coulomb distortion of intermediate states have been proposed [12,13], but they are obliged to employ further approximations for evaluating the transition-matrix elements. The accuracy of these secondary approximations is difficult to assess quantitatively. It is therefore desirable to investigate the effect of the Coulomb interactions in a rigorous manner.

In a recent Letter [18], we have presented the first *nonperturbative* quantum-mechanical calculations of the Thomas mechanism as an application of a general method to treat energetic ion-atom collisions. This method adopts the coupled-channel formalism; however, it avoids the numerical difficulties mentioned above by

using Gaussian-type orbitals (GTO), which allow for an analytical evaluation of the single-center as well as of the two-center matrix elements. While Gaussian basis expansions have been successfully used for a very long time in quantum chemistry [19] and recently for electron-molecule scattering [20] and positron formation [21], the application to ion-atom collisions has hardly been tried. The reason is that the extension to traveling orbitals needed for charge transfer entails the continuation of the standard methods to complex variables. Formulas for the matrix elements have been given by Errea, Mendez, and Riera [22], but only one practical application [23] is known to us. In this work, the interest is mainly focused on two-electron effects, namely, in $He^{2+}+He$ and $He^{+}+He^{+}$ collisions for energies up to 100 keV/u. Correspondingly, the number of GTO's per electron had to be kept rather small.

In Ref. [18] we have considered $p+H$ collisions at 5 MeV. Adopting the impact-parameter treatment with classical rectilinear trajectories for the projectile motion, we have performed two-center, coupled-channel calculations with a GTO basis, confining ourselves to s states. In this paper we investigate in more detail the dependence on the basis states and extend our calculations to larger basis sets including p and d states. In addition to $p+H$ collisions at 5 MeV, we also consider bombarding energies of 2.8 and 1 MeV.

In Sec. II we give a brief outline of the method and in Sec. III we present and discuss the results and compare them with other theoretical and with experimental differential cross sections. In Sec. IV we add some concluding remarks. Atomic units are used unless explicitly stated otherwise.

II. METHOD

We consider a process in which the target nucleus is located at a fixed origin and the projectile is moving along a classical trajectory $\mathbf{R}=\mathbf{b}+\mathbf{v}t$, where $\mathbf{b}$ is the impact parameter and $\mathbf{v}$ a constant velocity pointing in the positive z direction. We wish to solve the time-dependent Schrödinger equation,

$$\left[H-i\frac{\partial}{\partial t}\right]\Psi(\mathbf{r},t)=0 \tag{1}$$

by introducing an expansion

$$\Psi(\mathbf{r},t)=\sum_{i=1}^{N_T} a_i(t)\psi_i^T(\mathbf{r}_T,t)+\sum_{i=N_T+1}^{N} a_i(t)\psi_i^P(\mathbf{r}_P,t) \tag{2}$$

in terms of the target functions

$$\psi_i^T(\mathbf{r}_T,t)=\varphi_i^T(\mathbf{r}_T)e^{-iE_i^T t} \tag{3}$$

and the projectile functions

$$\psi_i^P(\mathbf{r}_P,t)=\varphi_i^P(\mathbf{r}_P)e^{-iE_i^P t}e^{i\mathbf{v}\cdot\mathbf{r}_T}e^{-i(1/2)v^2 t}\ . \tag{4}$$

Here, $\mathbf{r}_T,\mathbf{r}_P$ are the electron coordinates measured from the target and projectile nuclei, respectively, and φ_i^T,φ_i^P are the eigenfunctions of the target and projectile Hamiltonians with eigenvalues E_i^T and E_i^P. In Eq. (4), the last two exponentials are the translation factors for the origin chosen. The Schrödinger equation (1) is equivalent to a set of coupled equations which read in matrix form

$$i\underline{N}\dot{\mathbf{a}}=\underline{V}\mathbf{a}\ , \tag{5}$$

where $\underline{N}$ is the overlap matrix, $\mathbf{a}$ the vector of expansion coefficients, $\dot{\mathbf{a}}$ its time derivative, and $\underline{V}$ the interaction matrix with the elements

$$\begin{aligned} N_{ik}&=\langle\psi_i|\psi_k\rangle\ ,\\ V_{ik}&=\langle\psi_i|H-i\partial/\partial t|\psi_k\rangle\ . \end{aligned} \tag{6}$$

The labels may belong to the same center or to different centers T,P. The atomic eigenfunctions of each center are now expanded in Gaussian basis functions as

$$\varphi_{nlm}(\mathbf{r})=\sum_{\nu} c_\nu^{(nl)}e^{-\alpha_\nu r^2}r^l Y_l^m(\hat{\mathbf{r}})\ , \tag{7}$$

where the solid harmonics $r^l Y_l^m(\hat{\mathbf{r}})$ are written in Cartesian coordinates. Within this representation, the single-center matrix elements of each atomic Hamiltonian are calculated analytically and, subsequently, the atomic eigenfunctions and eigenenergies are obtained by numerical diagonalization.

Before performing the latter task, a choice has to be made for the Gaussian width parameters α_ν. As has been discussed by Gramlich, Grün, and Scheid [23], it is economical for computations to choose the width parameters in a geometrical progression, that is, $\alpha_{\nu+1}=\rho\alpha_\nu$. However, if one wishes to achieve a good representation of continuum states, one may adopt a factor of ρ which slowly varies with ν in such a way that large widths (small α_ν) are emphasized. For typical calculations, the range parameter $\bar{r}_\nu=(\alpha_\nu)^{-1/2}$ varies between $\bar{r}_{\min}=0.005$ and $\bar{r}_{\max}=20$ a.u.

Since all basis functions are square integrable, so are the eigenstates. By diagonalizing the atomic Hamiltonian for each center, we obtain bound states as well as a large number of states with positive eigenvalues. These states are interpreted as pseudostates which approximate the oscillating continuum wave functions up to a maximum range $\bar{r}_{\max}$ and then fall off. The positive-energy states hence represent wave packets produced by a superposition of adjacent continuum states in a certain energy interval. Among the eigenstates obtained from the matrix diagonalization, we usually keep only the lowest bound states. The eigenvalues for the two lowest principal shells are calculated with a precision of 10^{-14} or better, while the remaining bound-state eigenenergies have at least an accuracy of 10^{-12}. We found that this level of precision is important, because even a small contamination with continuum states gives rise to spurious contributions to bound-state capture. In addition to the high-lying bound states, we also discard those continuum states whose energies are too high above the resonant energy $E_m=\frac{1}{2}mv^2$ and, consequently, do not contribute to charge transfer. The numbers N_T and N_P (with $N_T+N_P=N$) of eigenstates included in the expansion (2) is much smaller than the number of Gaussian basis states

at each center.

When a basis of atomic eigenstates $\psi_i^{T,P}$ has been specified, the two-center matrix elements within the set of Eq. (6) are calculated for each value of b and of vt. At this point, the translation factor $\exp(i\mathbf{v}\cdot\mathbf{r}_T)$ enters in the determination of the matrix elements, and an analytical evaluation in terms of elementary functions is no longer possible. As has been pointed out by Errea, Mendez, and Riera [22], it is necessary to introduce a complex auxiliary function,

$$F_m(z)=\int_0^1 s^{2m}e^{-sz^2}ds=\tfrac{1}{2}z^{-m-1/2}\gamma(m+\tfrac{1}{2},z)\ , \quad (8)$$

where z is a complex variable, m a non-negative integer, and $\gamma(m+\frac{1}{2},z)$ is the incomplete γ function [24]. This function has to be evaluated with a very high accuracy. All matrix elements are expressed as multiple sums over either elementary expressions or expressions involving the function $F_m(z)$. The occurrence of multiple summations again requires a high numerical precision.

The matrix elements oscillate very rapidly as a function of $z=vt$. We therefore use 500 points (and for checks of convergence, 1000 points) in the half-space $vt<0$. By symmetry and interpolation, all additional values can be obtained. The number of basic points is much larger than needed for lower energies.

The coupled equations (5) are solved for the initial condition that at $t\rightarrow-\infty$, the occupation amplitude for the target ground state is $a_{T1s}=1$, while all other amplitudes are zero. Once we are in possession of the occupation amplitudes $a_k(b,t)$ for all states k, we can calculate the differential cross section in the center-of-mass system for capture from an initial state with magnetic quantum number m into a final projectile state k with magnetic quantum number m' as [25]

$$\frac{d\sigma_k}{d\Omega}=\left|i\mu v\int_0^\infty b^{2iv+1}a_k(b,t\rightarrow\infty)J_{|m-m'|}(\eta b)db\right|^2. \quad (9)$$

Here $\mu=M_TM_P/(M_T+M_P)$ is the reduced mass of target and projectile; $v=Z_TZ_P/v$; $\eta=2\mu v\sin(\theta/2)$; where θ is the scattering angle in the center-of-mass frame; and $J_{|m-m'|}$ denotes the Bessel function of the first kind. In the particular case of $p+H$ scattering with $M_T=M_P$, the cross section in the laboratory system is

$$\sigma_L(\theta_L)=4\cos\theta_L\,\sigma(\theta=2\theta_L)\ .$$

In order to examine the numerical procedure, numerous checks have been applied: (a) We compared the single-center and two-center matrix elements for $1s$, $2s$, $2p$, $3s$, $3p$, and $3d$ states with those calculated by one-dimensional integration according to the standard procedure, (see e.g., [26]). The results agree with each other for all digits valid for the computer program of Ref. [26]. (b) We compared the orientation parameters and dipole moments for $He^+(n=2)$ states in $He^{2+}+H$ collisions with those of Ref. [27]. The agreement includes phases and is almost perfect. (c) We also compared with the results of Ref. [28]. (d) Finally, we checked the validity of unitarity, detailed balancing, and symmetry with respect to the interchange between projectile and target states.

III. RESULTS AND DISCUSSION

The Thomas mechanism is usually visualized within second-order perturbation theory which, in turn, carries a close connection to the original classical picture [4]. Accordingly, the electron propagates freely in the intermediate state between the two collisions and, as a free continuum state, belongs equally to target and projectile. In contrast to this, in a two-center, coupled-channel treatment, one distinguishes two portions of the continuum: one centered around the target, the other centered around the projectile. Both of these continua are represented by a finite number of discretized states. Because of the limitation in their number, an overcompleteness cannot occur but, to some extent, the straightforward interpretability gets lost in a three-body Coulomb problem.

In Ref. [18] we have shown that in two-step transfer processes, we may identify two reaction sequences which carry most of the weight in the Thomas mechanism. In sequence A, the target electron is excited into a high-lying state of the target Coulomb continuum with energy $E_m=\frac{1}{2}m_ev^2$ corresponding to a free electron traveling with the same speed v as the projectile. From there, the electron is resonantly transferred into the projectile ground state. In the alternative sequence B, the electron is first transferred resonantly into a high-lying state (with energy E_m) of the projectile continuum and subsequently deexcited into the projectile ground state.

In our partial-wave treatment, the resonance occurs in energy and does not permit us to draw conclusions regarding the momentum transfer. Nevertheless, one may expect that in the target resonant state of sequence A, longitudinal momentum components prevail which point in the direction of the projectile motion, while in the projectile resonant state of sequence B, longitudinal momentum components dominate which point opposite to the direction of motion.

In Ref. [18] we have examined the Thomas mechanism for 5-MeV $p+H$ collisions in coupled-channel calculations with 25 $l=0$ eigenstates built from 40 GTO's at each target and projectile. In the present paper, we considerably increase the number of s states, also include p and d states, and furthermore extend calculations to 2.8- and 1-MeV projectile energy.

A. Collisions of 5-MeV protons with hydrogen

We have chosen the energy of 5 MeV for the most detailed calculations because experimental data and various theoretical calculations are available. The resonant energy is $E_m=\frac{1}{2}m_ev^2=100.8$ a.u. The mesh of Gaussian scale parameters α_i in our calculations is chosen so that one of the eigenvalues is close to E_m. Similarly as in the earlier calculations [18], we find that this state carries considerable weight in the target as well as in the projectile. In Fig. 1 we show the weighted impact-parameter-dependent transfer probability

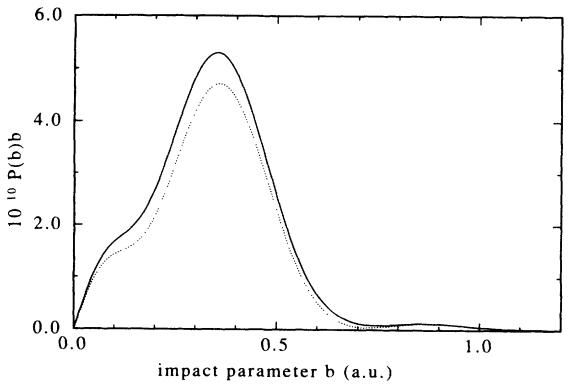

FIG. 1. Weighted impact-parameter dependence of the transfer probability for $p+H$ collisions at 5 MeV described by a basis set ($T34s/P34s$). Solid line, capture into the $1s$, $2s$, and $3s$ bound states; dotted line, capture into the $1s$ state only.

$$P(b)b = |a(b,t\rightarrow\infty)|^2 b$$

for a basis set, denoted by ($T34s/P34s$), consisting of 34 s states *at each of target and projectile.* This set of eigenstates is constructed from 85 GTO's and comprises $1s$, $2s$, and $3s$ bound states and 31 continuum states, the highest of which has an energy of 131 a.u. The scale parameters of the GTO basis vary in a modified geometric progression so that the corresponding radii $\bar{r}$ range from $\bar{r}_{\min}=1.1\times10^{-4}$ to $\bar{r}_{\max}=20$ a.u. The dotted curve in the figure denotes $1s$-$1s$ transitions, while the solid curve indicates capture into all bound states. The calculations are converged within the subspace of s states. Neither the addition of further s states nor the choice of a different set of GTO's changes the results.

Figure 2 shows the differential cross section obtained from Eq. (9) for the basis set of Fig. 1. For comparison, we also include the experimental data of Vogt *et al.* [17] and, as a dashed line, the coupled-channel calculations in which only $1s$, $2s$, and $3s$ bound states at target and projectile are included. We see that the coupled-channel calculations without continuum states completely fail to yield a structure resembling a Thomas peak. Furthermore, the cross section at forward angles, i.e., the total cross section, is largely overestimated. These results are not unexpected. It has been shown by Toshima, Ishihara, and Eichler [29] that the results of two-state, coupled-channel calculations tend to those of a first-order distorted-wave approximation (denoted by DWBA1) as the energy increases, and both converge to those of the Oppenheimer-Brinkmann-Kramers (OBK) approximation. Since the addition of further bound states does not change the situation, it was concluded [29] that solutions of close-coupling calculations always "converge to the OBK value unless the basis includes continuum states through which the Thomas double-scattering process may occur." Indeed, with the inclusion of continuum states, the dotted and the solid curves for the $1s$-$1s$ and the summed differential cross sections show a clear Thomas peak structure, although the height of the peak is somewhat underestimated compared to the experimental data. When comparing with the experimental data, we have to take into consideration the finite angular resolution of the detector. The theoretical results actually should be folded with the experimental resolution, as we have done in Ref. [18]. In the present paper, we only present unfolded theoretical results in order to preserve the full theoretical information.

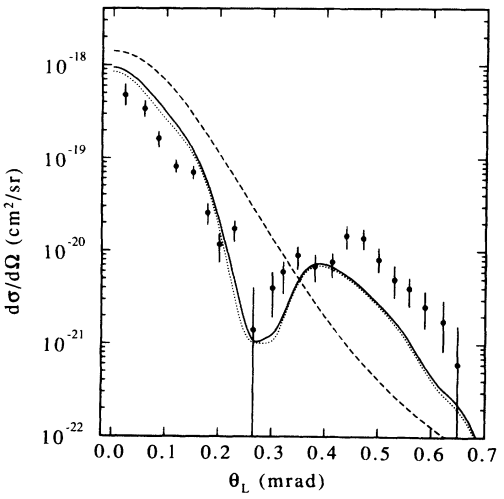

FIG. 2. Differential cross section for electron capture in $p+H$ collisions at 5 MeV using the basis set ($T34s/P34s$) of Fig. 1. Solid line, capture into the $1s$, $2s$, and $3s$ bound states; dotted line, capture into the $1s$ state only; dashed line, only $1s$, $2s$, and $3s$ bound states are included in the expansion (2) for the coupled-channel calculations.

At first sight, it may appear surprising that the Thomas mechanism, which is classically associated with severe geometrical restrictions, should be reproduced by target and projectile s states alone. However, since the classical electron-projectile impact parameter b_e is related to the electron scattering angle θ by $b_e=(Z_P/v^2)\cot(\theta/2)$, the classical electron-projectile angular momentum may be estimated as

$$l=vb_e=(Z_P/v)\cot(\theta/2)=\sqrt{3}Z_P/v \qquad (10)$$

for the Thomas mechanism. In the present case, with $Z_P=1$ and $v=14.1$, we have a classical angular momentum of $l=0.12$. The same argument holds for the electron-target interaction. This suggests that the lowest partial waves at target and projectile should be sufficient to represent the effect.

In the calculations leading to Fig. 3, we have augmented the basis set by 57 p states (a number which includes the magnetic substates) at the target, expanded in terms of 75 GTO's. We hence have a basis of 91 eigenstates at the target and 34 at the projectile, in our notation ($T34s,57p/P34s$). At the target, 9 bound states are included, namely, $1s$, $2s$, $2p$, $3s$, and $3p$, while at the projectile we have bound $1s$, $2s$ and $3s$ states. As resonant states with energy close to $E_m=100.8$ a.u., we have s and p states at the target and s states at the projectile. If continuum p states are included at both centers, difficulties arise to reach a satisfactory convergence. These prob-

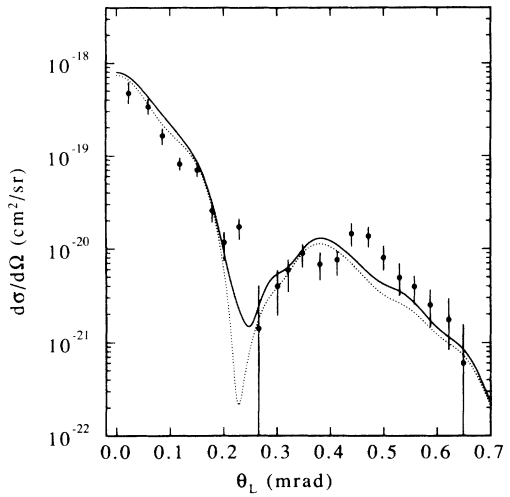

FIG. 3. Differential cross section for electron capture in $p+H$ collisions at 5 MeV using the basis set ($T34s,57p/P34s$). Solid line, capture into the $1s$, $2s$, and $3s$ bound states; dotted line, capture into the $1s$ state only.

lems are now being investigated. With only one p continuum, however, we find that our calculations are essentially converged. Figure 3 shows that the inclusion of p states does not drastically change the picture in comparison to Fig. 2. The height of the Thomas peak is increased, while the forward cross section is decreased, both effects bringing the theoretical results into closer agreement with the experimental data.

In the calculation for Fig. 4 , we have augmented the basis set of Fig. 3 by 30 d states, so that we have the set ($T34s,57p,30d/P34s$). The s, p, and d states are expanded on 85, 75, and 66 GTO's, respectively. The target bound states now include all hydrogenic bound states up

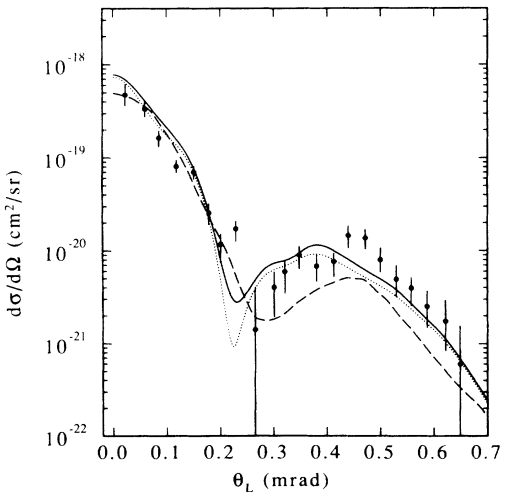

FIG. 4. Differential cross section for electron capture in $p+H$ collisions at 5 MeV using the basis set ($T34s,57p,30d/P34s$). Solid line, capture into the $1s$, $2s$, and $3s$ bound states; dotted line, capture into the $1s$ state only; dashed line; second-order Born approximation calculations [11]. The experimental data are from Vogt *et al.* [17].

to the $n=3$ shell, while the highest continuum state reaches to the energy of 135 a.u. The accuracy of the calculated eigenenergies for $n=3$ is 10^{-14} and better by one or two orders of magnitude for the lower shells. As has been pointed out before, this accuracy is important in order to avoid contamination with continuum states. It is seen that the differential cross sections do not change too much compared to Fig. 3. The dip in the cross section has become shallower but, on the whole, the comparison reveals that a certain convergence has been reached. In Fig. 4 we also show results from $B2B0$ calculations (dashed curve) [11,14] in which Coulomb boundary conditions are satisfied. It should be pointed out that the calculated Thomas peak occurs at an angle slightly below the classical Thomas angle $\Theta_{Th}=0.47$ mrad in the laboratory system. This small shift is mainly due to the fact that continuum states are attached to both centers. If only one-center continuum states are used, the peak position comes closer to the classical Thomas angle Θ_{Th} [18]. The superposition onto a strongly sloping first-order curve is another cause of the shift.

It is instructive for coupled-channel calculations to follow the time development of the system for a given impact parameter by plotting $P_k(b,t)=|a_k(b,t)|^2$ as a function of $z=vt$. For our present purpose, we have chosen $b=0.28$ a.u., which is close to the maximum of $P(b)$, (see Fig. 1). In order to limit the number of states, we have selected the basis set ($T34s/P34s$) of Figs. 1 and 2. Figure 5 displays the occupation probability of the target states (upper diagram) and of the projectile states (lower diagram). When interpreting the curves, it should be kept in mind that the basis states belonging to different

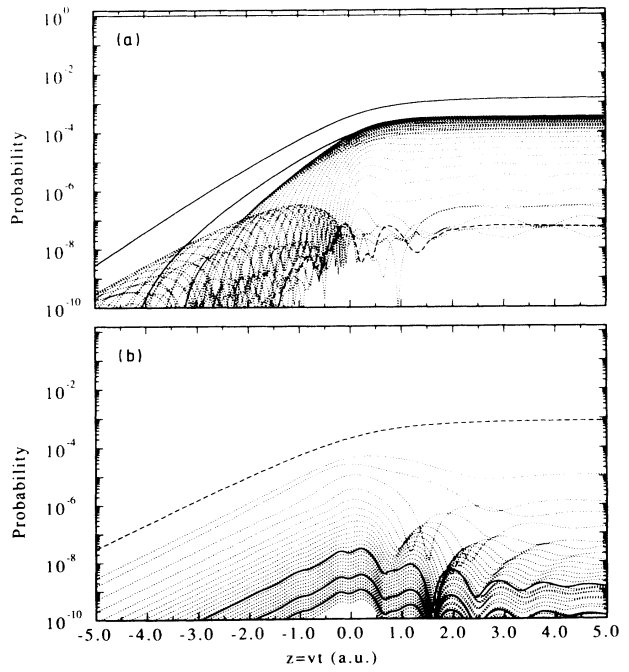

FIG. 5. Time evolution of the occupation probabilities of (a) target states and (b) projectile states in $p+H$ collisions at 5 MeV. Solid curves, bound states; dashed curves, resonant continuum states; dotted curves, other continuum states.

centers are not strictly orthogonal to each other. Nevertheless, the probability interpretation holds to a good approximation. For example, the overlap between the resonant target state and a projectile bound state is a few 10^{-2} (both for the real and the imaginary part) at $vt=1$ and a few 10^{-3} at $vt=5$.

In Fig. 5 bound states, both at target and at projectile, are indicated by solid lines, the resonant continuum state by a dashed line, and all other continuum states by dotted lines. Looking at the excited target states first, we observe that the low-lying ($2s$ and $3s$) target states are most strongly populated, followed by the low-lying continuum states. The accumulation of lines for the low continuum is related to the fact that the density of continuum states is much higher for the low-lying states than for the high-lying states. Thus, for low positive energies, each line represents a small piece of the continuum, while at high energies, each state represents a larger energy interval. In any case, it is seen that target ionization mainly occurs into the low-energy portion of the continuum.

In the projectile frame, the resonant state (i.e., the energy interval it represents) has by far the highest occupation probability. Since, by momentum overlap, the backward-directed momentum components within the projectile resonant state are expected to carry a large weight, the associated continuum electrons are interpreted as resulting from target ionization. In contrast, the low-lying projectile continuum states give rise to "electron capture into the continuum." The projectile bound states are populated by couplings among bound states (as may be verified by a calculation with bound states only) and by the strong coupling with the target resonant state whose contribution reduces the occupation probability by a factor of about 2. This is in accordance with the results of Fig. 2. Qualitatively, we have predominantly excitation of low-lying states in the target and capture into high-lying states of the projectile.

The total transfer cross sections in 5-MeV $p+H$ collisions for the set ($T34s,57p,30d/P34s$) corresponding to Fig. 4 are

$$\sigma(1s)=2.23\times10^{-26}\ \text{cm}^2\ ,$$

$$\sigma(2s)=3.14\times10^{-27}\ \text{cm}^2\ ,$$

and

$$\sigma(3s)=8.66\times10^{-28}\ \text{cm}^2\ .$$

The sum is

$$\sigma_{\text{theor}}=2.63\times10^{-26}\ \text{cm}^2$$

as compared to the experimental value [30] of

$$\sigma_{\text{exp}}=3.1\times10^{-26}\ \text{cm}^2$$

for capture into all bound states.

B. Collisions of 2.8-MeV protons with hydrogen

We have also performed calculations for the collision energy of 2.8 MeV for which experimental [17] and theoretical [15] data are available. The resonant energy is $E_m=56.45$ a.u. Because of the lower energy compared to the 5-MeV case, we expect an improved convergence of the expansion. Indeed, we reach a satisfactory convergence for the data set ($T33s,36p,25d/P33s$), where the s states are constructed from 85 GTO's, the p states from 75 GTO's, and the d states from 74 GTO's with $\bar{r}_{\min}=1.2\times10^{-4}$ (for s states) and $\bar{r}_{\max}=20$ a.u. This set includes $1s$, $2s$, $2p$, $3s$, and $3p$ bound states at the target and $1s$, $2s$, and $3s$ bound states at the projectile, while the highest continuum state has an energy of 96 a.u.

In Fig. 6 we present the calculated differential cross section. The solid line again denotes capture into the final $1s$, $2s$, and $3s$ states, while the dotted line describes capture into the final $1s$ state only. For comparison, we include the results from second Born calculations (dashed line) by Toshima and Igarashi [15], which are obtained by multiplying the calculated $1s$-$1s$ cross section with a factor of 1.2 in order to account for contributions from higher projectile states. The experimental data are from Vogt *et al.* [17]. It is seen that the coupled-channel calculations yield a Thomas peak which is less pronounced than at 5-MeV proton energy. In the second Born calculation [15], the Thomas peak is still visible, while the possible peak structure of the experimental results depends on a single data point at 0.38 mrad. If this point is disregarded, one observes at most a shoulder in the cross-section curve. In any case, the theoretical curves of the present coupled-channel calculation and the second-order Born approximation seem to disagree consistently with the experimental results [17]. On the other hand, the strong potential Born (SPB) and the continuum-distorted-wave (CDW) cross sections, both of which are

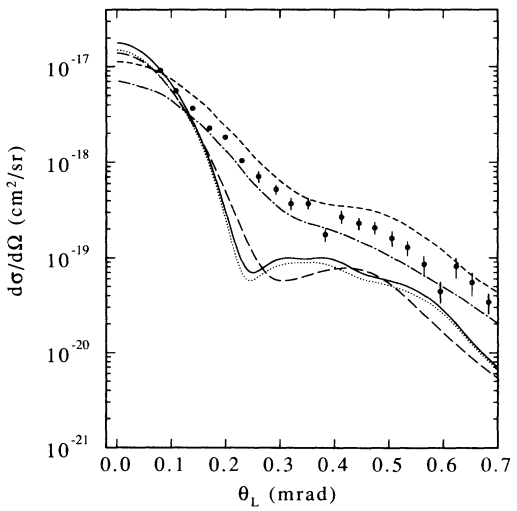

FIG. 6. Differential cross section for electron capture in $p+H$ collisions at 2.8 MeV using the basis set ($T33s,36p,25d/P33s$). Solid line, capture into the $1s$, $2s$, and $3s$ bound states; dotted line, capture into the $1s$ state only; dashed line, the second-order Born approximation calculations [15]; short-dashed line, the strong potential Born approximation [13] (folded with the experimental resolution) taken from [17]; dot-dashed line, the continuum-distorted-wave approximation [12] (folded with the experimental resolution) taken from [17]. The experimental data are from Vogt *et al.* [17].

folded with the experimental resolution, yield a cross section similar to the experimental one. Regarding the coupled-channel calculations, we should mention that one gets almost identical results if the d states are omitted.

The total transfer cross sections in 2.8-MeV $p+H$ collisions for the set ($T33s,36p,25d/P33s$) corresponding to Fig. 6 are

$$\sigma(1s)=5.50\times10^{-25}\ \text{cm}^2\ ,$$

$$\sigma(2s)=7.24\times10^{-26}\ \text{cm}^2\ ,$$

and

$$\sigma(3s)=1.86\times10^{-26}\ \text{cm}^2\ .$$

Experimental total transfer cross sections are not available at this energy.

C. Collisions of 1-MeV protons with hydrogen

We finally consider the case of 1-MeV collision energy, corresponding to $E_m=20.2$ a.u. In Fig. 7, we present the differential cross section for the data set ($T24s,24p,20d/P24s$) with 70 GTO's for s states, 64 GTO's for p states, and 60 GTO's for d states, and $\bar{r}_{\min}=9.8\times10^{-5}$ a.u. (for s states) and $\bar{r}_{\max}=20$ a.u. This set includes $1s$, $2s$, $2p$, $3s$, $3p$, and $3d$ bound states at the target and $1s$, $2s$, and $3s$ states at the projectile, while the highest continuum state has an energy of 28 a.u. At this energy, the coupled-channel calculations yield a shoulder in the differential cross section (the solid and dotted lines stand for total and $1s$ capture, respectively), while the second Born results [15] (dashed line) show a much weaker shoulder. Experimental data are not available at this energy.

The total transfer cross sections in 1-MeV $p+H$ collisions for the set ($T24s,24p,20d/P24s$) corresponding to Fig. 7 are

$$\sigma(1s)=1.92\times10^{-22}\ \text{cm}^2\ ,$$

$$\sigma(2s)=2.42\times10^{-23}\ \text{cm}^2\ ,$$

and

$$\sigma(3s)=7.75\times10^{-24}\ \text{cm}^2\ .$$

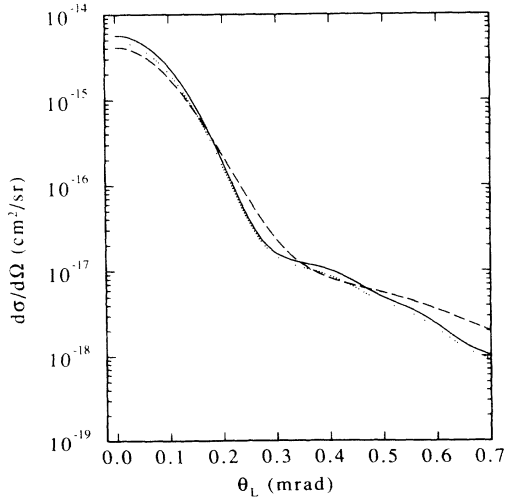

FIG. 7. Differential cross section for electron capture in $p+H$ collisions at 1 MeV using the basis set ($T24s,24p,20d/P24s$). Solid line, capture into the $1s$, $2s$, and $3s$ bound states; dotted line, capture into the $1s$ state only; dashed line, second-order Born approximation calculations [15].

IV. CONCLUDING REMARKS

We have presented differential and total cross sections derived from extensive and systematic coupled-channel calculations for electron transfer in proton-hydrogen collisions at 5, 2.8, and 1 MeV. It has been our aim to investigate the Thomas mechanism in an approach that takes all Coulomb interactions among the three charges fully into account. In doing so, we have demonstrated in detail that the nonperturbative coupled-channel method can be efficiently extended to high-lying continuum states by expanding atomic eigenstates (in our case up to angular momenta $l=2$) in terms of a sufficiently large basis set of Gaussian-type orbitals. Although these orbitals are localized in space, we are able to accurately represent the oscillatory behavior of the continuum wave functions as far away from the atomic centers as 20 K-shell radii.

The study of the time development of occupation probabilities during the collision shows that among the target states the bound and the low-lying continuum states are most strongly excited, while at the projectile, it is the resonant (high-lying) continuum state that is dominantly populated. Nevertheless, via coupling among states, both the target and the projectile resonant continuum states contribute equally to the charge transfer. In fact, we have explicitly shown that the inclusion of continuum states in the basis set is crucial for producing a Thomas peak. The role of the resonant projectile state is in accord with the usual classical and second-order Born approximation picture of the Thomas mechanism. The classical picture with its severe geometrical restrictions is also consistent with the fact that already spherical s states describe most of the effect, with p and d states giving rise only to modifications. This is so because the relative classical angular momenta between electron and projectile or target are very small for the specific kinematics of the Thomas double-scattering mechanism. The results of a large number of calculations show satisfactory convergence and yield good agreement with experimental data at 5 MeV but not at 2.8 MeV.

Although there are some features that need further investigation and extensions have to be made to asymmetric collision systems, we believe that the method presented here is suitable for providing further insight into the dynamics of the three-body Coulomb problem even at high collision energies.

V. ACKNOWLEDGMENTS

The authors appreciate helpful discussions with C. L. Cocke and are greatly indebted to Y. Awaya for providing computing time at the RIKEN computer.

*Also at: Fachbereich Physik, Freie Universität Berlin, D-1000 Berlin 33, Germany.

[1] D. R. Bates and R. McCarroll, Proc. R. Soc. London, Ser. A **245**, 175 (1958).

[2] See, e.g., W. Fritsch and C. D. Lin, Phys. Rep. **202**, 1 (1991).

[3] See, e.g., M. R. C. McDowell and J. P. Coleman, *Introduction to the Theory of Ion-Atom Collisions* (North-Holland, Amsterdam, 1970).

[4] L. H. Thomas, Proc. R. Soc. London, Ser. A **114**, 561 (1927).

[5] R. Shakeshaft and L. Spruch, Rev. Mod. Phys. **51**, 369 (1979).

[6] N. Toshima, Phys. Rev. A **42**, 5739 (1990); **45**, R2663 (1992).

[7] R. M. Drisko, Ph.D. thesis, Carnegie Institute of Technology, 1955.

[8] P. J. Kramer, Phys. Rev. A **6**, 2125 (1972).

[9] P. R. Simony and J. H. McGuire, J. Phys. B **14**, L737 (1981); P. R. Simony, J. H. McGuire, and J. Eichler, Phys. Rev. A **26**, 1337 (1982); J. M. Wadehra, R. Shakeshaft, and J. Macek, J. Phys. B **14**, L767 (1981); J. E. Miraglia, R. D. Piacentini, R. D. Rivarola, and A. Salin, *ibid.* **14**, L197 (1981).

[10] D. P. Dewangan, *Electronic and Atomic Collisions,* edited by H. B. Gilbody *et al.* (North-Holland, Amsterdam, 1988), p. 425; D. P. Dewangan and B. H. Bransden, J. Phys. B **21**, L353 (1988).

[11] D. Belkic, Europhys. Lett. **7**, 323 (1988); Phys. Rev. A **43**, 4751 (1991).

[12] I. M. Cheshire, Proc. Phys. Soc. London **84**, 89 (1964); J. S. Briggs, P. T. Greenland, and L. Kocbach, J. Phys. B **15**, 3085 (1982); J. Macek and X. Y. Dong, Phys. Rev. A **38**, 3327 (1988); S. Alston, *ibid.* **42**, 331 (1990).

[13] J. Macek and S. Alston, Phys. Rev. A **26**, 250 (1982); J. Macek, *ibid.* **37**, 2365 (1988); J. Macek and R. O. Barrachina, Comments At. Mol. Phys. **24**, 287 (1990); J. Macek, J. Phys. B **18**, L71 (1985); H. Marxer and J. Briggs, Z. Phys. D **13**, 75 (1989); K. Taulbjerg, R. O. Barrachina, and J. Macek, Phys. Rev. A **41**, 207 (1990).

[14] F. Decker and J. Eichler, J. Phys. B **22**, L95 (1989); **22**, 3023 (1989).

[15] N. Toshima and A. Igarashi, Phys. Rev. A **45**, 6313 (1992).

[16] E. Horsdal-Pedersen, C. L. Cocke, and M. Stöckli, Phys. Rev. Lett. **50**, 1910 (1983).

[17] H. Vogt, R. Schuch, E. Justiniano, M. Schulz, and W. Schwab, Phys. Rev. Lett. **57**, 2256 (1986).

[18] N. Toshima and J. Eichler, Phys. Rev. Lett. **66**, 1050 (1991).

[19] S. F. Boys, Proc. R. Soc. London, Ser. A **200**, 542 (1950); H. Taketa, S. Huzinaga, and K. Oohata, J. Phys. Soc. Jpn. **21**, 2313 (1966); E. Clementi and G. Corongiu, Chem. Phys. Lett. **90**, 359 (1982).

[20] B. M. Nestmann and S. D. Peyerimhoff, J. Phys. B **23**, L773 (1990).

[21] R. N. Hermit, C. J. Noble, and B. H. Bransden, J. Phys. B. **23**, 4185 (1990).

[22] L. F. Errea, L. Mendez, and A. Riera, J. Phys. B **12**, 69 (1979).

[23] K. Gramlich, N. Grün, and W. Scheid, J. Phys. B **22**, 2567 (1989).

[24] *Handbook of Mathematical Functions,* edited by M. Abramowitz and I. A. Stegun (Dover, New York, 1965).

[25] D. Belkic, R. Gayet, and A. Salin, Phys. Rep. **56**, 279 (1979).

[26] K. Fujiwara and N. Toshima, J. Phys. Soc. Jpn. **52**, 4118 (1983).

[27] N. Toshima, R. Shingal, and C. D. Lin, J. Phys. B **25**, L11 (1992).

[28] W. Fritsch (private communication).

[29] N. Toshima, T. Ishihara, and J. Eichler, Phys. Rev. A **36**, 2659 (1987).

[30] W. Schwab, G. B. Baptista, E. Justiniano, R. Schuch, H. Vogt, and E. W. Weber, J. Phys. B **20**, 2825 (1987).

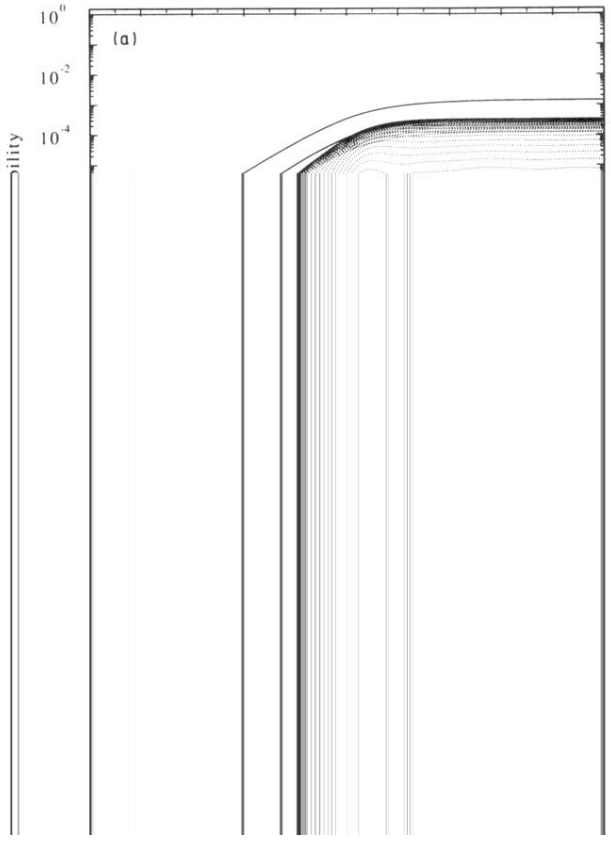
10^{0}
10^{-2}
10^{-4}
ility
(a)